J. Vis. Commun. Image R. 48 (2017) 281–291

Contents lists available at ScienceDirect

J. Vis. Commun. Image R.

journal homepage: www.elsevier.com/locate/jvci

Detecting image seam carving with low scaling ratio using multi-scale spatial and spectral entropies ☆

Dengyong Zhang [a,b], Ting Yin [a], Gaobo Yang [a,*], Ming Xia [a], Leida Li [c], Xingming Sun [d]

[a] School of Information Science and Engineering, Hunan University, Changsha 410082, China
[b] School of Computer and Communication Engineering, Changsha University of Science and Technology, Changsha 410114, China
[c] School of Information and Control Engineering, China University of Mining and Technology, Xuzhou 221116, China
[d] School of Computer and Software, Nanjing University of Information Science and Technology, Nangjing 210044, China

ARTICLE INFO

Article history:
Received 28 November 2016
Revised 22 May 2017
Accepted 16 July 2017
Available online 20 July 2017

Keywords:
Image forensics
Content-aware image retargeting
Seam carving
Low scaling ratios
Spatial and frequency entropy
Object removal

ABSTRACT

Seam carving is the most popular content-aware image retargeting technique. However, it may also be used to correct poor photo composition in photography competition or to remove object from image for malicious purpose. A blind detection approach is presented for seam carved image with low scaling ratio (LSR). It exploits spatial and spectral entropies (SSE) on multi-scale images (candidate image and its down-sampled versions). We observe that when a few seams are deleted from an original image, its SSE distribution is greatly changed. Forty-two features are designed to unveil the statistical properties of SSE in terms of centralized tendency, dispersion tendency and distribution tendency. They are combined with the local binary pattern (LBP)-based energy features to form ninety-six features. Finally, support vector machine (SVM) is exploited as classifier to determine whether an image is original or suffered from seam carving. Experimental results show that the proposed approach achieves superior detection accuracy over the state-of-the-art works, especially for resized image by seam carving with LSRs. Moreover, it is robust against JPEG compression and seam insertion.

1. Introduction

With the popularity of powerful image editing tools, people without any knowledge about image processing can easily fake a photo in a visually plausible way. There is a growing number of tampered images flooding over televisions, magazines and Internet. This breaks our traditional concept of "seeing is believing" and brings serious crises to public confidence [1,2]. Evaluating the authenticity of digital images has become a crucial issue in the community of image information security. In the past years, both active and passive methods have been developed for this purpose. Digital watermarking [3] and hashing [4] are known as active techniques, which are applicable mainly in a controlled environment since pre-processing is required for them. Fortunately, digital image forensics has been emerged to detect image forgery [5,6]. Since passive image forensics approaches do not require any pre-embedded watermark or pre-generated hashing, they have wider usages in practical forensics scenarios.

Content-aware image resizing (CAIR) has attracted extensive research interests to adapt image on diverse display terminals. Among the existing CAIR techniques, seam carving [7] is the most popular one for its excellent performance. A seam is an optimal 8-connected path of pixels either from top to bottom, or left to right, in which the optimality is defined by an energy function. By repeatedly deleting or inserting seams with the lowest energies, an image is easily resized without leaving any visually noticeable artifacts. Thus, seam carving has been adopted by Adobe Photoshop CS5 and GIMP as adaptive scaling to improve image quality for aesthetic purpose [8]. However, if the resultant image is used for photo competition, it is actually a cheating since the composition of a photo may be corrected with seam carving. Moreover, seam carving can also be used for object removal [9], which is usually malicious. As shown in Fig. 1, the girl who is hanging her hand with a man is deliberately removed. Apparently, this might have changed the semantic content that the image delivers. Therefore, it is worthy of investigation to design a blind detector capable of exposing the resized images after seam carving. Until now, only a few approaches have been reported for seam carving forgery detection. Inspired by the similarities between image forensics and image steganalysis, Sarkar et al. [10] made the first attempt of seam carving detection by exploiting the Shi-324 Markov features,

☆ This paper has been recommended for acceptance by Zicheng Liu.

* Corresponding author.
E-mail address: yanggaobo@hnu.edu.cn (G. Yang).

http://dx.doi.org/10.1016/j.jvcir.2017.07.006
1047-3203/

(a) (b) (c)

Fig. 1. An example of seam carving for object removal [9]: (a) original image; (b) marked object to be removed; (c) final image after object removal.

yet its detection accuracy is below 77.3%. Fillion et al. [11] proposed a seam carving detection approach by exploiting a set of image features such as wavelet absolute moments. Its detection accuracy is up to 91.3% when 30% seams are removed. Later, Wei et al. [12] proposed a patch analysis method to detect seam carved images. Candidate images are firstly divided into 2×2 blocks, which is referred to be mini-squares. Then, one type is searched from nine types of patches that is most likely to recover a mini-square from seam carving. The patch transition probability among three-connected mini-squares is exploited to improve its detection accuracy. In addition, Ryu et al. [13] exploited energy bias and noise to unveil the traces of seam carving. Motivated by the fact that local binary pattern (LBP) is an excellent local texture descriptor, we presented an improved detection approach to [13] by extracting energy bias and noise features in LBP domain [14]. It improves the detection accuracy up to 98.66% when 30% seams are removed. For seam-carved forgery detection in JPEG images, Liu et al. [15] proposed an improved approach with Calibrated Neighboring Joint Density (CNJD) by exploiting the similarities between image steganalysis and seam-carved forgery detection. Recently, Kanoksak et al. [16] proposed a tamper detection approach for JPEG images with seam modifications. It exploits blocking artifact characteristics matrix (BACM) to reflect the symmetry of blocking effect in normal JPEG image.

The aforementioned works have achieved notable success in exposing seam carving forgery with high scaling ratios (HSRs), in which HSR refers to a scaling ratio that is bigger than 10%. However, we believe that the detection of seam-carved forgery with low scaling ratios (LSRs) is worthy of more research efforts. The reasons behind this are two-folds. First, since more seams are deleted from original image for seam carving with a HSR, it implies that the original image is more likely to be over-squeezed. Thus, there are often visually unpleasant distortions such as global structural distortion in resized images. Users might easily perceive seam-carved forgery even without the aid of passive forensics. This has been verified by existing approaches that higher detection accuracies are achieved for seam carving with the increasing of scaling ratio. Second, global geometric distortion, local texture deformation and information loss are three side effects that affect the perceptual quality of retargeted images [17]. For seam carved images with LSRs, there usually exist no global geometric distortion and local texture deformation. Thus, information loss is a more feasible clue to expose seam-carved forgery with a LSR. Unluckily, information loss is extremely difficult to be measured without the original image as reference. Therefore, the detection of seam carving forgery with LSRs is much more challenging. Actually, this is the underlying reason behind the fact that it is still in scarcity of robust detector for seam-carved forgery with LSRs.

In Shannon's information theory, entropy is a measure of the unpredictability of information. Image entropy indicates the amount of information contained within an image. Lots of works reveal the relationships among image entropy, histogram, image moments and perceived image quality, which verify that image entropy captures the statistical information of image over scales [18]. Moreover, natural images are highly structured in the sense that their pixels exhibit strong dependencies in both spatial and frequency domain. These dependencies convey important information about image content. Motivated by the success of image entropy in image quality assessment [19,20], we make the first attempt to address the detection of seam-carved forgery with LSRs from image entropy point of view. Specifically, local spatial and spectral entropies (SSE) on multi-scale images are exploited for blind forensics. The inherent reasons are two-folds. First, when an image is subject to seam carving, the amount of information is reduced. Second, human visual system (HVS) exhibits multi-scale property when perceiving an image, and the hierarchical structures are contained in the scale space representation of digital image [20]. Our preliminary experiments also show that when a few seams are carved, there are great change of local image entropies for those blocks near carved seams, which will be illustrated later. To expose the change of local entropy, forty-two SSE features are designed for multi-scale images from three levels: centralized tendency, dispersion tendency and distribution tendency. They are combined with our earlier energy bias based features in LBP domain [14] to form ninety-six features. Finally, support vector machine (SVM) is exploited as pattern classifier to decide whether an image is original or suffered from seam carving. Experimental results show that the proposed approach achieves superior detection accuracy over the state-of-the-art works, especially for seam carved images with LSRs. Moreover, it is also effective for seam inserting detection and robust against JPEG compression.

The rest of this paper is organized as follows: Section 2 briefly introduces seam carving and analyze the traces that might be exploited as clues for blind forensics. Section 3 presents forensics feature extraction. Experimental results are reported in Section 4 and we conclude this paper in Section 5.

2. Image seam carving

Seam carving was originally presented as a CAIR technique [7–9]. A seam is an optimal 8-connected path of pixels on a single image either from top to bottom, or left to right, in which the optimality is defined by an energy function. For an image I of size $n\times m$, a vertical seam is defined by

$$\mathbf{s}^{\mathbf{v}} = \{I, col(i)\}_{i=1}^{n}, s.t.\forall i, |col(i) - col(i-1)| \leqslant 1 \quad (1)$$

where i and col(i) are the row and column coordinates, respectively. By repeatedly removing seam with the lowest energy,image resizing is achieved while preserving important image content. Each pixel's energy is measured by an energy function e as follows:

$$e(I) = \left|\frac{\partial}{\partial x}I\right| + \left|\frac{\partial}{\partial y}I\right| \quad (2)$$

From the energy function e of a pixel, the energy of a vertical seam $E(s)$ is defined as follows:

$$E(s) = \sum_{i=1}^{n} e(i, col(i)), s.t.\forall i, |col(i) - col(i-1)| \leqslant 1 \quad (3)$$

After constructing a cumulative minimum energy matrix M for all connected paths, a vertical seam with the lowest energy $s^* = minE(s)$ is located via dynamic programming.

$$M(i,j) = e(i,j) + \min(M(i-1,j-1), M(i-1,j), M(i-1,j+1)) \quad (4)$$

When removing a seam from an image, all the pixels at the right side of this seam are shifted left to fill the missing path. That is, the possible visual artifacts of removing a seam merely occur near the removed seam, leaving the rest image intact. Fig. 2 shows image seam carving with two scaling ratios of 3% and 30%. When the scaling ratio is 3%, all the seams to be deleted pass through the gaps between cars, as shown in Fig. 2(b). The resized image keeps well most important content without any visually noticeable artifacts. When the scaling ratio is 30%, the seams pass through the gaps between cars and cross the cars as well, as shown in Fig. 2(d). Since the seams are not uniformly distributed, there are some geometric distortions [21,22] such as the twists of yellow park lines, as shown in Fig. 2(e). This type of visually annoying artifact can be easily perceived by naked eyes, which implies users can know possible forgery without the aid of passive forensics. Thus, the blind detection of seam carving with LSRs is more technically challenging, simply because information loss is its primary side effect. This motivates us to exploit information loss as an important clue for the passive detection of seam carving with LSRs.

3. Proposed blind forensics approach

Fig. 3 is the framework of the proposed seam carving forgery detection approach. Similar to most existing blind forensics approaches, it consists of two key steps, i.e., feature extraction and classification. As mentioned in the previous section, information loss is a crucial clue for the blind detection of seam carving with LSRs. Meanwhile, seam carving achieves image resizing by successively deleting seams with low energies, which inevitably changes the energy distribution within the image. Thus, the energy-based feature is also beneficial for seam carving forgery detection. In this paper, both local information loss and global energy distribution are fully considered to design statistical features for blind forensics. Specifically, local SSE-based features are defined on multi-scale images to expose the information loss caused by seam carving. Moreover, the energy bias-based features

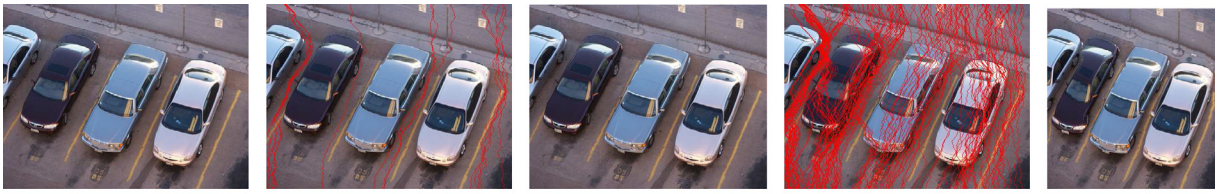

(a) (b) (c) (d) (e)

Fig. 2. Seam carving with different scaling ratios: (a) an original image; (b) original image with 3% vertical seams; (c) 3% carved image; (d) original image with 30% vertical seams; (e) 30% carved image.

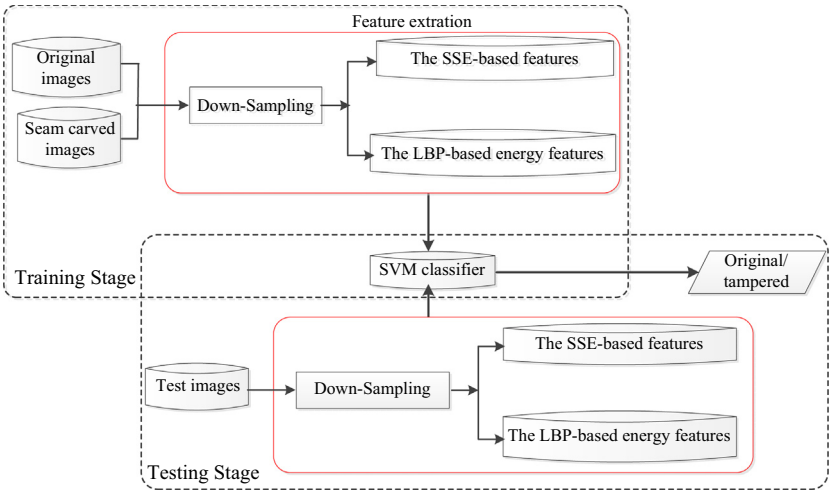

Fig. 3. Proposed framework based on the SSE-based features and the LBP-based features.

in our earlier work [14] are exploited for classification, which are combined with the SSE-based features to improve detection accuracy. The proposed detection approach is also a machine learning-based scheme. In the training stage, sufficient natural images are adopted and resized by seam carving to generate tampered images. Then, these resized images are down-sampled with a factor of 2 for multi-scale analysis and cropped with factors of half and two-thirds for energy analysis. That is, there are 3 multi-scale images and 3 cropped images for each seam-carved image, respectively. Then, the SSE-based features and the LBP-based energy features are extracted from seam-carved images and their multi-scale images for training. In the testing stage, the same statistical features are extracted from candidate/suspicious images and then input into SVM for final classification.

3.1. Multi-level statistical features based on spatial and spectral entropy

Seam carving does not lead to any common artifacts such as blur or ghosting shadow, because only those pixels along vertical or horizontal seams are removed without changing any grey-scale values of the rest pixels. Let us take a vertical seam as example. The intuitive change is that those pixels at the right side of the carved seam are shifted one pixel left to fill in the gap. Nevertheless, there is still local information loss near this seam. That is, local information loss is the main artifact of seam carving, especially when the scaling ratio is low. Moreover, the dependencies among adjacent pixels are changed for those pixels near the carved seam. Since natural image exhibits strong dependencies among its adjacent pixels in both space and frequency domain, local information loss is addressed from local SSE point of view as follows.

3.1.1. Local image entropy

Image entropy indicates the amount of information contained in an image. When image entropy is computed over multi-scales, it reveals the statistical entropy of scale space [31]. Since seam carving with LSRs mainly leads to local information loss, local image entropy [32,33] is exploited to measure the loss of local information and the change of pixel dependencies for carved images. For an image of size $M \times N$, its entropy is defined as follows:

$$E = -\sum_{i=0}^{L-1} P_i log P_i \tag{5}$$

where $P_i = \frac{n_i}{M \times N}$ is the probability of grayscale i appears in the image, L is the maximal grayscale, and n_i is the number of pixels with grayscale i. If we define a local region Ω_k within the image by a window of size $M_k \times N_k$, then the local entropy of Ω_k can be defined similarly in which $P_j = \frac{n_j}{M_k \times N_k}$ is the probability of grayscale j appears in the neighborhood Ω_k, and n_j is the number of pixels with grayscale j in the neighborhood. When a vertical seam is removed, all the pixels at its right side are shifted one pixel left to fill in the gap of the removed seam. This implies that the 8×8 blocks at the right side are re-organized, which makes their local entropies quite different from their original ones. Fig. 4 shows the changes of local entropy when four seams are continuously carved, which are marked with red, green, blue and yellow, respectively. For simplicity, a 64×64 block of the original image is enlarged to show the influence of continuously carved seams towards the local entropies of those blocks at right side of those seams. Fig. 4 shows the differences of local entropies between the original 64×64 block and its carved block, in which a "jet" colormap is used to represent the degree of differences. From the figure, we observe that there are obvious changes of local entropies for those blocks at the right side of those carved seam, even though only four seams are carved. To analyze the behavior of seam carving with LSRs, we further compare their local entropy histogram, as shown in Fig. 5. For the first original image, it has a continuous local entropy histogram with mean 4. Moreover, it is typically left-skewed, which means that there are less data at the left side of the mean value than the right side, leading to a longer tail at the left side. For the resized images, there are great changes of its distribution tendency. For the second image, it exhibits the same trend, but the change is more significant. Therefore, local image entropy is sensitive to seam carving with LSRs, which implies that local image entropy is an appropriate clue to expose the local information loss caused by seam carving with LSRs.

3.1.2. Multi-scales features of spatial entropy

For a given image, seam carving with different scaling ratios produces resized images with different spatial resolutions. Moreover, several works have revealed the relationships between image entropy, histogram and image moments, which verify that image entropy can capture image statistical information over scales [19,20]. In this paper, we firstly sub-sample each candidate image into 3 scales (low, middle and high). Then, seven statistical features are extracted from each scale image, which are summarized in Table 1. These features describe the spatial entropy distribution from three levels including centralized tendency, dispersion tendency and distribution tendency. Therefore, there are totally $7 \times 3 = 21$ features extracted from each candidate image.

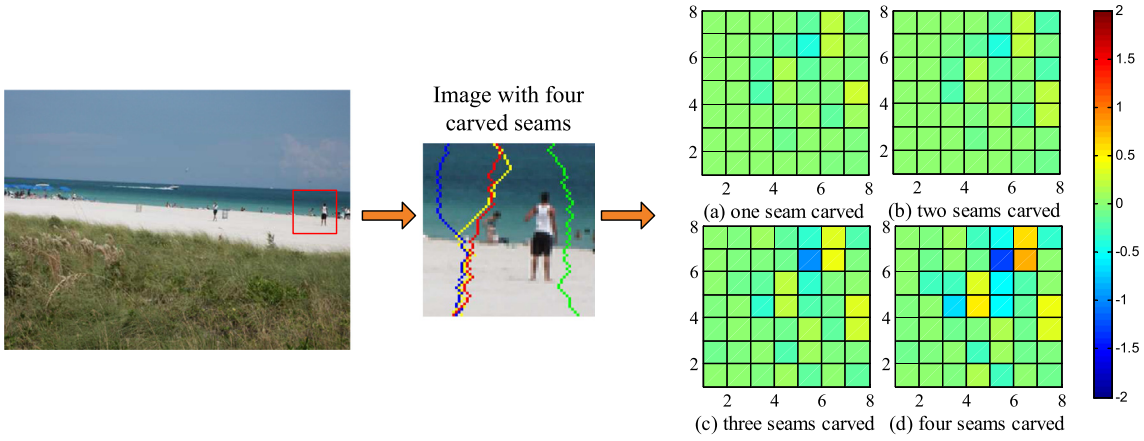

Fig. 4. An example of the local entropy changes when continuously carved four seams.

(a) Original image

(b) Original image

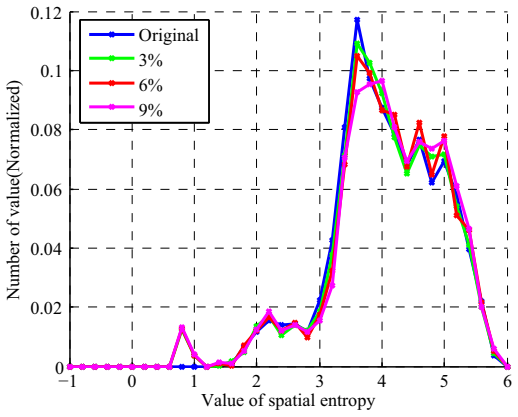

(c) Local entropy histogram with the scaling ratios of 3%, 6% and 9%

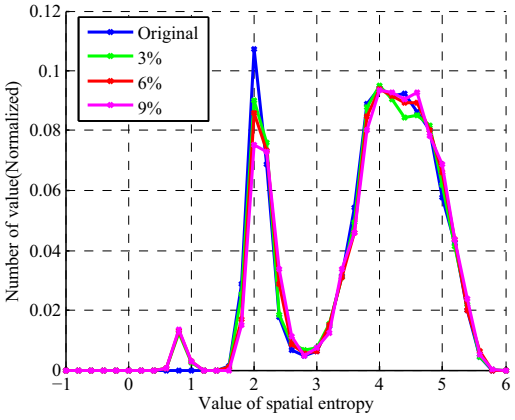

(d) Local entropy histogram with the scaling ratios of 3%, 6% and 9%

Fig. 5. Histograms of spatial entropies for seam carved images with LSRs.

Table 1
Seven statistical features based on local entropy histogram *E*.

Type	Features	Description
Centralized tendency	Mean	$\frac{1}{M\times N}\sum_{u=1}^{M}\sum_{v=1}^{N}E(u,v)$
	Median	The middle value in a set of ordered local entropy values
	Mode	The value that appears most frequently in a set of local entropy values
Dispersion tendency	Variance	$\frac{1}{M\times N}\sum_{u=1}^{M}\sum_{v=1}^{N}(E(u,v)-E_{mean})$
	Variable coefficient	$\frac{E_{mean}}{\sqrt{E_{variance}}}$
Distribution tendency	Skewness	$\frac{1}{M\times N}\sum_{u=1}^{M}\sum_{v=1}^{N}\left(\frac{E(u,v)-E_{mean}}{\sqrt{E_{variance}}}\right)^3$
	Kurtosis	$\frac{1}{M\times N}\sum_{u=1}^{M}\sum_{v=1}^{N}\left(\frac{E(u,v)-E_{mean}}{\sqrt{E_{variance}}}\right)^4$

3.1.3. Multi-scales features of spectral entropy

Spatial entropy reflects the probability distribution of local pixel values, while spectral entropy decribes the probability distribution of local DCT coefficients. Moreover, it has been proved that there exists a strong relationship between frequency entropy and the type of distortions [13]. To improve the robustness against post-processing such as JPEG compression, the definition of image entropy is extended to DCT domain. Firstly, we compute the DCT coefficient matrix *F* for each 8×8 block. Then, we generate a frequency probability map by normalizing the DCT coefficients as follows:

$$M(i,j) = \frac{D(i,j)^2}{\sum_i \sum_j D(i,j)^2} \tag{6}$$

where $1 \leqslant i, j \leqslant 8$, and $i, j \neq 1$ (DC is excluded), $D(i, j)$ is the DCT coefficient within a block. Then, the local spectral entropy is defined as follows:

$$E_{frequency} = -\sum_i \sum_j M(i,j)\log_2 M(i,j) \tag{7}$$

Similar to the spatial entropy, seven features (summarized in Table 1) are also extracted from each scale image to describe the distribution of spectral entropy. Thus, there are also $7 \times 3 = 21$ spectral entropy features. Fig. 6 compares the local spectral entropies among the original image, seam carved images with LSR (15 seams are carved from the original image) in TIFF and JPEG formats. Apparently, the untouched image has a continuous spectral entropy histogram, which is also "left-skewed". However, seam carving changes this distribution tendency to some extent. "JPEG" decreases the mean and changes the distribution, whereas there is just a little difference for TIFF image when it is compared with the original images histogram. Compared with the spatial entropy histogram, the spectral entropy histogram more clearly distinguishes the carved images in JPEG format. That is, the spectral entropy is an excellent descriptor of images'energy spectrum,

because it emphasizes the main frequency and main orientations within a local patch. From Figs. 5 and 6, we further observe that the entropy distributions of "JPEG" can be more easily distinguished from that of the original image. The reason behind this is that JPEG compression removes some high frequency signal from the original image, which decreases both spatial and spectral entropy.

3.2. LBP-based energy features

The above SSE-based features are specially designed for the blind detection of seam carving with LSRs. In practical forensics cases, users usually do not know whether a candidate image is seam carved or not, let alone the scaling ratio is either high or low. Thus, an ideal detector specially designed for seam carved forgery should be robust to scaling ratio. In our earlier work [14], it has been demonstrated that the energy, noise and seam-based features are effective for seam carving forgery detection, especially for those resized images with HSRs. Moreover, these features are extracted in LBP domain, instead of the conventional pixel domain to highlight local texture changes caused by seam carving [14]. Thus, these features are also exploited here to improve detection accuracy and robustness. To keep the readability and self-intact of this paper, these LBP-domain features are also summarized in Table 2. For detailed information, please refer to [14]. Due to the diversities of image contents, seams may locate in only part of the image. Therefore, we extract these 18 features from three scaled images including the half-resolution image, two-thirds resolution image and the whole image. That is, there are totally 54 LBP-based features $(18 \times 3 = 54)$ in this paper, which are combined with the SSE-based features for seam carving forgery detection.

3.3. SVM classifier for passive forensics

Blind image forensics is actually a binary decision between original images and forgery images. After extracting the 96 features (54 LBP-based features + 21 spatial entropy features + 21 spectral entropy features) from multi-scale images, a pattern classifier is exploited to decide whether a suspicious image is seam-carved or not. In this paper, the conventional support vector machine (SVM) is adopted for classification. SVM is a widely-used supervised learning method for its simplicity. In the training phase, two classes of images (original images and seam-carved images) are represented by the aforementioned feature vectors. Then, SVM finds an optimal linear decision surface, which is referred to be maximum margin hyper plane, by maximizing the geometric margin between the closest instances on either side. To further improve detection accuracy, feature vectors are non-linearly projected into a high dimensional feature space with the Radial Basis Function (RBF) kernel. In the final classification stage, feature vectors extracted from a candidate image are input into the trained SVM, and the image is classified as: seam-carved or non-carved.

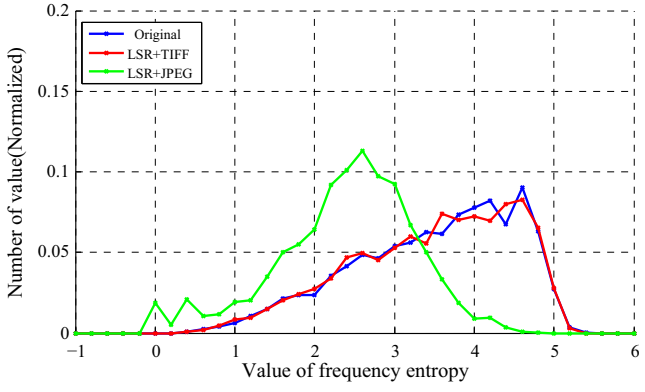

Fig. 6. Histograms of frequency entropy values for LSRs.

Table 2
Statistical features based on image I, noise level image N and cumulative minimum energy matrix M.

Type	Features	Description
Energy	Average column energy	$\frac{1}{m\times n}\sum_{i=1}^{m}\sum_{j=1}^{n}\lvert\frac{\partial}{\partial x}I(i,j)\rvert$
	Average row energy	$\frac{1}{m\times n}\sum_{i=1}^{m}\sum_{j=1}^{n}\lvert\frac{\partial}{\partial y}I(i,j)\rvert$
	Average energy	$\frac{1}{m\times n}\sum_{i=1}^{m}\sum_{j=1}^{n}(\lvert I\frac{\partial}{\partial x}(i,j)\rvert+\lvert\frac{\partial}{\partial y}I(i,j)\rvert)$
	Average energy difference	$\frac{1}{m\times n}\sum_{i=1}^{m}\sum_{j=1}^{n}(\lvert\frac{\partial}{\partial x}(i,j)\rvert-\lvert\frac{\partial}{\partial y}I(i,j)\rvert)$
Noise	Mean	$\frac{1}{m\times n}\sum_{i=1}^{m}\sum_{j=1}^{n}N(i,j)$
	Standard deviation	$\sqrt{\frac{1}{m\times n}\sum_{i=1}^{m}\sum_{j=1}^{n}(N(i,j)-N_{mean})^2}$
	Skewness	$\frac{1}{m\times n}\sum_{i=1}^{m}\sum_{i=1}^{n}(\frac{N(i,j)-N_{mean}}{\sqrt{N_{std}}})^3$
	Kurtosis	$\frac{1}{m\times n}\sum_{i=1}^{m}\sum_{i=1}^{n}(\frac{N(i,j)-N_{mean}}{\sqrt{N_{std}}})^4$
Seam	$\text{Verticalseam}_{max}$	$\max_{i=1}^{m}M(i,n)$
	$\text{Verticalseam}_{min}$	$\min_{i=1}^{m}M(i,n)$
	$\text{Verticalseam}_{mean}$	$\frac{1}{m}\sum_{i=1}^{m}M(i,n)$
	$\text{Verticalseam}_{std}$	$\sqrt{\frac{1}{m}\sum_{i=1}^{m}(verticalseam_{mean}-M(i,n))^2}$
	$\text{Verticalseam}_{diff}$	$verticalseam_{\max}-verticalseam_{\min}$
	$\text{Horizontalseam}_{max}$	$\min_{i=1}^{n}M(m,i)$
	$\text{Horizontalseam}_{min}$	$\min_{i=1}^{n}M(m,i)$
	$\text{Horizontalseam}_{mean}$	$\frac{1}{n}\sum_{i=1}^{n}M(m,i)$
	$\text{Horizontalseam}_{std}$	$\sqrt{\frac{1}{n}\sum_{i=1}^{n}(horisontalseam_{mean}-M(m,i))^2}$
	$\text{Horizontalseam}_{diff}$	$\sqrt{\frac{1}{n}\sum_{i=1}^{n}(horisontalseam_{mean}-M(m,i))^2}$

4. Experimental results and analysis

4.1. Experimental environment setup

To evaluate the performances of the proposed approach, extensive experiments are conducted on a personal computer (PC). The hardware configurations are summarized as follows: Intel(R) Core(TM) i5-2450M CPU @ 2.5 GHz, 4.0 GB RAM, 200G hard disk. The proposed detector is implemented with MATLAB 7.0 on a Windows XP system. SVM is directly downloaded from [23], and Radial Basis Function (RBF) is used as the kernel function. Optimal kernel parameters are found via grid search, and a fourfold cross validation strategy is exploited. Moreover, Python and Gnuplot are used for parameter optimization.

To the best of our knowledge, there is no open image database specially designed for seam-carved forgery detection. Thus, we build the test image database for experiments by ourselves. Firstly, two image databases including UCID and UCUS are chosen. The UCID dataset is an uncompressed color image database, which consists of 1338 TIFF images with a variety of contents including natural scenes and man-made objects, both indoors and outdoors [24]. The UCUS database is an "Unknown Compression/Undefined Source and Size" image database, which contains 1009 JPEG images at unknown QF from several sources in different sizes. To evaluate the performances of seam carved forgery detection, we then build three image sets from the original images in the UCID and UCUS databases, respectively. For the first test image set, it is built to test the detection accuracy of simple seam carving. The 1338 images in the UCID database are resized by seam carving with 9 scaling ratios, which are 1%, 3%, 5% 7%, 9%, 10%, 20%, 30% and 50%, respectively. Thus, there are totally $1338 \times (9 + 1)$ images including the original images and the retargetted images. For the second test

Table 3
Three test image sets for performance evaluation.

Test image set	Image database	Processing method	Number of result images
Test set 1	UCID(1338)	Seam carving with 9 different scaling ratios	1338(9 + 1) = 13380
Test set 2	UCID(1338) and UCUS(1009)	(1) The UCID database are compressed into JPEG images with QFof 75, which are combined with the 1009 JPEG images of the UCUS image database; (2) the 1338 + 1009 JPEG images are decompressed and resized with 7 scaling ratios including 1%, 2%, 5%, 10%, 20%, 30% and 50%; (3) the resized images are re-encoded into JPEG images again with five QFs of 10, 20, 50, 75 and 100, respectively	(1338 + 1009)(75 + 1) = 84,492
Test set 3	UCID(1338) and UCUS(1009)	Similar to the second test image set, but the images are enlarged by inserting seams, instead of deleting seams in the process of seam carving	(1338 + 1009)(75 + 1) = 84,492

Table 4
Comparison of detection accuracy (%) for LSR seam carving without post-processing.

Scaling factor	Accuracy (%)				
	Patch-based [12]	Energy-based [13]	LBP-based [14]	BACM-based [16]	Proposed method
1%	47.90	45.10	37.33	**63.39**	62.37
3%	50.75	50.90	55.53	53.51	**94.88**
5%	46.15	54.82	67.08	55.94	**94.96**
7%	52.00	58.26	76.05	67.64	**84.15**
9%	59.23	61.36	78.34	55.38	**90.28**
10%	57.91	65.22	80.00	63.36	**92.04**
20%	74.18	75.37	94.48	61.36	**96.97**
30%	91.34	85.52	98.66	73.65	**99.03**
40%	89.70	91.94	**99.85**	78.92	**99.85**
50%	94.93	96.27	99.85	88.00	**99.93**

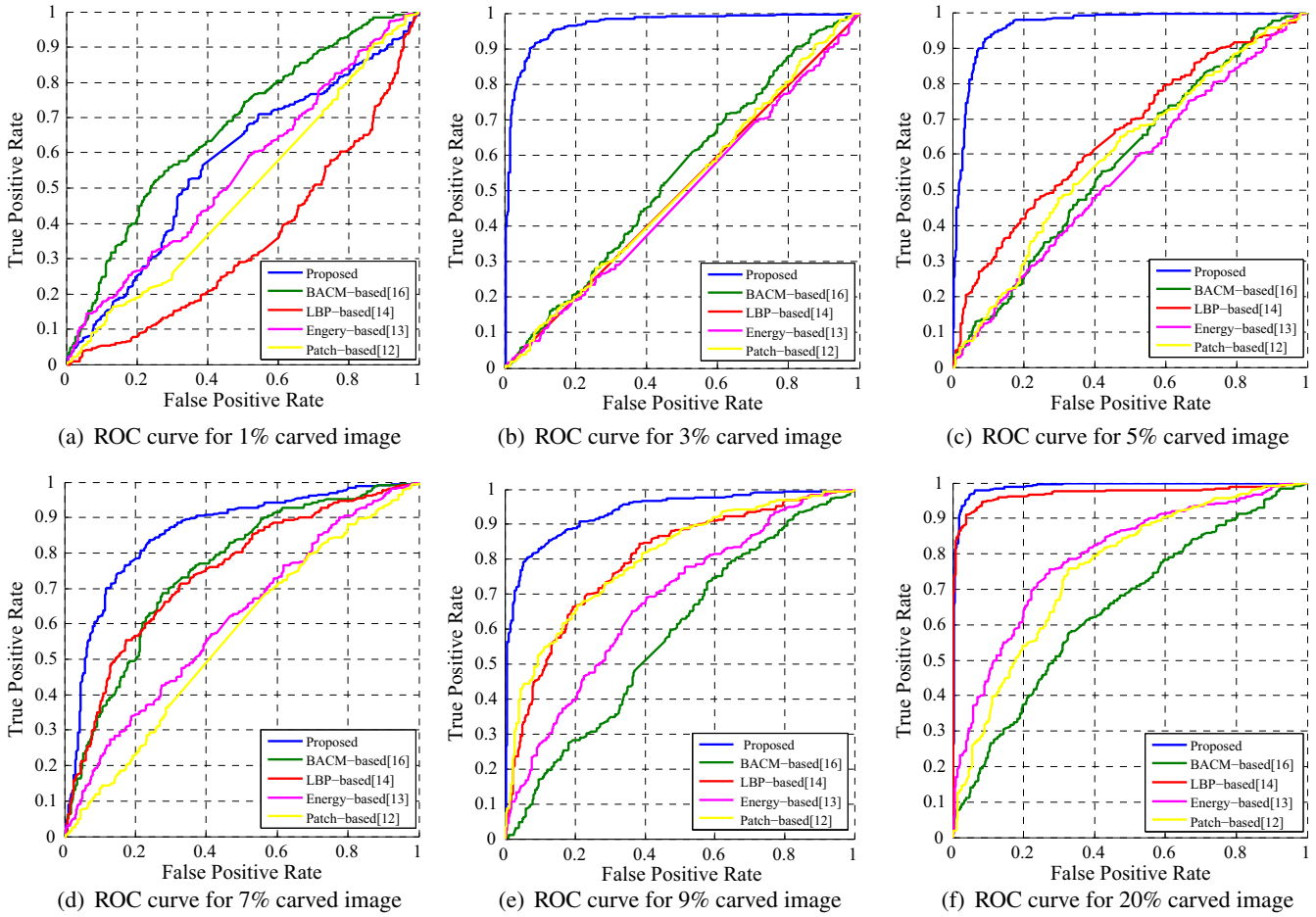

(a) ROC curve for 1% carved image (b) ROC curve for 3% carved image (c) ROC curve for 5% carved image

(d) ROC curve for 7% carved image (e) ROC curve for 9% carved image (f) ROC curve for 20% carved image

Fig. 7. Comparison of ROC curves.

Table 5
Comparison of detection accuracy (%) for seam carving at different tampered ratio and quality factor.

Scaling factor	QF10	QF20	QF50	QF75	QF100	QF10	QF20	QF50	QF75	QF100
(a1) LBP-based method [14] (UCID database)						*(a2) LBP-based method [14] (UCUS database)*				
1%	98.24	95.14	81.05	43.27	42.79	99.46	98.41	82.90	43.06	40.68
2%	98.54	95.03	82.32	47.46	47.50	99.55	98.07	84.79	45.79	44.90
5%	98.43	95.40	86.85	64.42	63.34	99.55	98.17	88.16	61.84	63.18
10%	98.32	95.29	87.70	64.28	65.47	99.60	98.07	90.39	68.58	67.05
20%	98.24	96.26	92.03	78.96	89.97	99.60	98.46	95.24	93.10	82.26
30%	98.99	97.83	96.82	91.74	92.56	99.85	99.36	98.22	95.44	95.44
50%	99.22	98.43	91.85	95.78	95.81	99.7	99.21	**99.71**	97.67	97.37
(b1) BACM-based method [16] (UCID database)						*(b2) BACM-based method [16] (UCUS database)*				
1%	97.98	95.48	87.11	**71.04**	**91.03**	98.71	97.23	88.7	**73.79**	**94.25**
2%	98.17	95.4	84.12	64.72	92.49	98.51	96.98	87.27	67.00	**95.94**
5%	98.24	94.73	82.92	69.25	95.48	98.12	96.09	84.59	69.23	97.32
10%	97.5	94.13	82.32	78.77	97.38	98.56	95.29	84.24	81.82	**98.91**
20%	97.23	90.7	78.44	85.16	98.8	98.02	93.56	81.52	86.37	**99.6**
30%	96.26	87.44	83.52	92.53	99.18	97.82	91.23	85.88	93.06	**99.85**
50%	96.34	96.19	98.51	99.07	99.78	97.57	96.18	98.22	99.06	**100**
(c1) Proposed method (UCID database)						*(c2) Proposed method (UCUS database)*				
1%	**99.66**	**99.36**	**98.43**	62.37	89.13	**99.80**	**99.26**	**98.22**	61.36	88.13
2%	**99.78**	**99.44**	**98.32**	**85.35**	**96.00**	**99.80**	**99.36**	**97.94**	**83.22**	95.39
5%	**99.70**	**99.29**	**99.91**	**96.90**	**98.65**	**99.90**	**99.41**	**98.32**	**95.25**	**98.22**
10%	**99.63**	**99.59**	**99.85**	**91.26**	**98.61**	**99.90**	**99.45**	**98.56**	**91.67**	97.23
20%	**99.48**	**99.48**	**99.70**	**95.70**	**99.22**	**99.90**	**99.45**	**99.06**	**94.96**	98.56
30%	**99.55**	**99.70**	**99.74**	**99.51**	**99.74**	**99.90**	**99.75**	**99.45**	**99.31**	99.75
50%	**99.85**	**99.85**	**99.85**	**99.74**	**99.81**	**99.90**	**99.80**	**99.71**	**99.80**	99.90

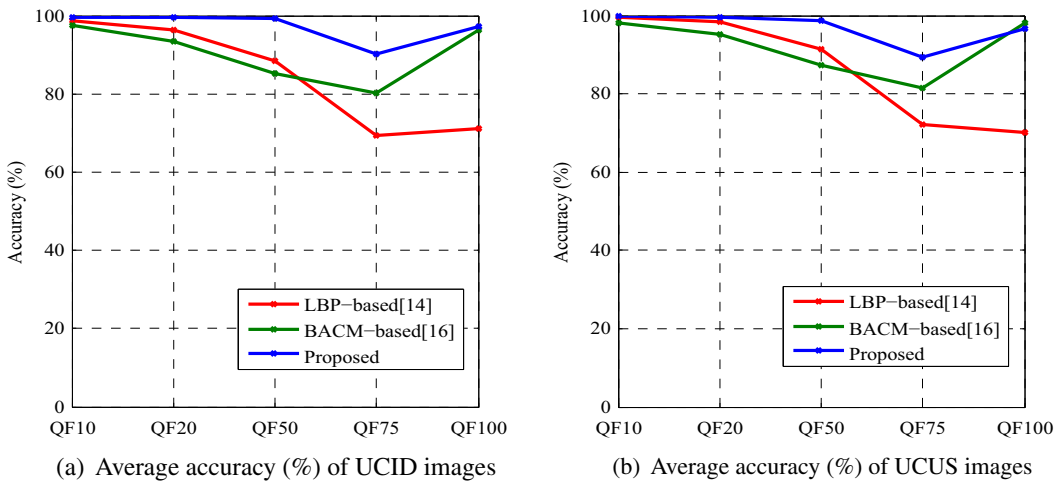

(a) Average accuracy (%) of UCID images (b) Average accuracy (%) of UCUS images

Fig. 8. Average accuracy of tampered JPEG images with different QFs.

image set, it is to test the detection accuracy of seam carved images with further JPEG compression. The 1338 images in the UCID database are firstly compressed into JPEG images with QF of 75, which are combined with the 1009 JPEG images from the UCUS image database. Then, the 1338 + 1009 JPEG images are decompressed and resized with 7 scaling ratios including 1%, 2%, 5%, 10%, 20%, 30% and 50%. Finally, the resized images are re-encoded into JPEG images with five QFs of 10, 20, 50, 75 and 100, respectively. Thus, there are totally $(1338 + 1009) \times (7 \times 5 + 1) = 84{,}492$ images including the original images and the retargetted images after JPEG compression. For the third test image set, it is specially designed for the detection of image enlargement by seam insertion with further JPEG compression. Its building procedure is quite similar to the second test image set, but the images are enlarged by inserting seams, instead of seam carving for image shrinkage. Table 3 summarizes these three test image sets for performance evaluation. Please note that the second and the third test image sets are the same with the test image sets used in [10]. To make fair comparisons with the existing approaches, four state-of-the-art works are chosen as baselines. They are denoted as the patch-based method [12], the energy-based method [13], the LBP-based method [14] and the BACM-based method [16], respectively. Thus, there are totally five detectors including the proposed detector for performance comparisons. Please note that they are tested with the same test image set under the same hardware and software environment.

4.2. Results of seam carved forgery detection

Experiments are conducted on three test image sets, respectively. That is, both image shrinkage and image enlargement by seam carving are separately tested, and the resized images with further JPEG compression are also tested. To ensure the randomness of our experiments, a 4-fold cross validation strategy is exploited. That is, each test image set is divided into four subsets with equal amount of images. Three subsets are used for training and the rest subset is used for testing. The detection experiments

Table 6
Comparison of detection accuracy (%) for seam insertion and JPEG compression.

Scaling ratio	QF10	QF20	QF50	QF75	QF100	QF10	QF20	QF50	QF75	QF100
(a1) LBP-based method [14] (UCID database)						*(a2) LBP-based method [14] (UCUS database)*				
1%	98.39	94.96	79.04	42.86	45.22	99.41	98.02	80.82	40.73	45.69
2%	98.43	95.07	79.045	45.00	49.78	99.65	97.87	91.96	41.92	51.19
5%	98.65	95.74	84.83	61.55	67.38	99.5	98.22	84.39	57.98	66.25
10%	98.62	95.40	83.22	55.68	59.15	99.45	98.17	82.06	54.96	57.88
20%	98.77	95.81	85.35	61.90	65.78	99.40	98.07	85.33	61.94	65.91
30%	98.62	96.00	86.85	68.57	71.30	99.45	98.17	87.86	69.92	71.70
50%	99.01	97.12	91.85	84.04	89.50	99.50	98.66	90.33	79.73	84.84
(b1) BACM-based method [16] (UCID database)						*(b2) BACM-based method [16] (UCUS database)*				
1%	98.17	95.63	88.64	73.06	88.94	98.72	96.93	89.2	75.77	91.92
2%	98.24	95.59	88.30	66.52	89.91	98.81	96.93	90.73	71.75	92.52
5%	98.24	96.15	88.71	69.69	92.60	98.72	97.23	90.88	73.49	**95.29**
10%	98.66	96.94	92.15	76.53	96.00	98.96	97.92	93.21	79.73	97.52
20%	98.58	97.46	95.18	85.02	98.32	98.91	98.22	96.68	87.36	**99.06**
30%	98.84	98.17	97.09	90.47	99.18	99.06	98.76	97.77	93.26	**99.41**
50%	99.33	98.77	98.73	95.63	99.40	99.26	99.45	98.82	97.23	**99.85**
(c1) Proposed method (UCID database)						*(c2) Proposed method (UCUS database)*				
1%	**99.78**	**99.66**	**98.43**	**96.00**	**98.43**	**99.9**	**99.36**	**97.82**	**95.19**	**97.08**
2%	**99.70**	**99.66**	**98.32**	**93.50**	**97.16**	**99.85**	**99.50**	**97.22**	**91.63**	**96.18**
5%	**99.81**	**99.36**	**96.60**	**78.21**	**95.33**	**99.85**	**99.36**	**96.13**	**77.30**	95.09
10%	**99.78**	**99.55**	**97.53**	**89.56**	**98.13**	**99.80**	**99.40**	**96.63**	**86.92**	**98.17**
20%	**99.81**	**99.81**	**98.77**	**94.15**	**99.14**	**99.85**	**99.35**	**98.36**	**94.49**	99.01
30%	**99.85**	**99.78**	**98.69**	**94.92**	**99.33**	**99.95**	**99.6**	**98.51**	**95.00**	99.21
50%	**99.90**	**99.93**	**99.48**	**97.72**	**99.60**	**99.90**	**99.45**	**99.21**	**98.17**	99.65

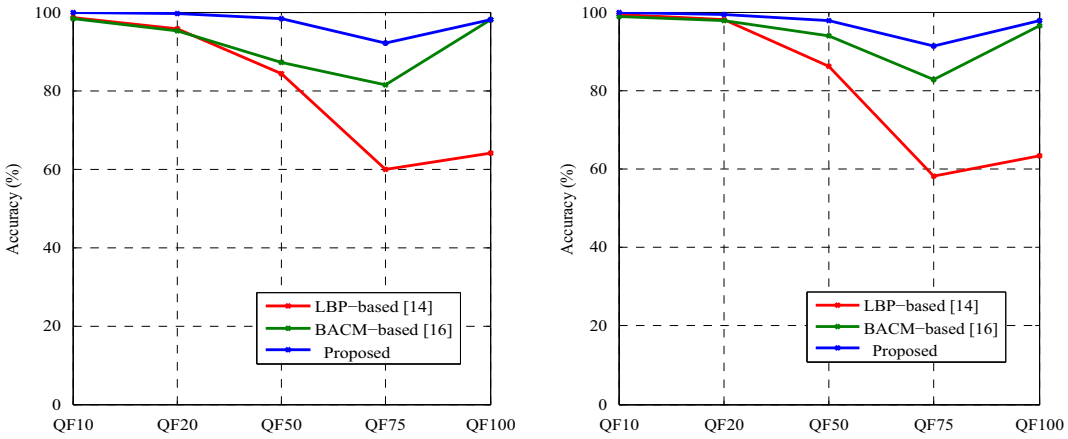

(a) Average accuracy (%) of UCID images (b) Average accuracy (%) of UCUS images

Fig. 9. Average accuracy of tampered images after seam insertion and JPEG compression with different QFs.

are repeated five times, and the average accuracy is reported as the final detection accuracy.

4.2.1. Seam carving with LSRs and no post-processing

Table 4 compares the detection accuracies of five detectors when are tested on the test image set 1. For each scaling ratio, the best detection accuracy is highlighted in bold. From Table 4, the proposed approach achieves the best detection accuracies for almost all scaling ratios, and they are on average about 25.03%, 22.97%, 12.73% and 25.33% higher than those of the patch-based method [12], the energy-based method [13], the LBP-based method [14] and the BACM-based method [16], respectively. For seam carved forgery with HSRs, the BACM-based method [16] has much lower detection accuracies than other four approaches, simply because it exploits the symmetric property of blocking artifacts of JPEG compression, which is not evident for uncompressed images. For the patch-based detector [12], it only considers the optimal type of patches for each mini-square by similarity comparison. That is, it does not explicitly consider local texture deformation and information loss due to seam carving. Thus, its detection accuracies are relatively lower, especially for those resized images with LSRs. Ryu et al. [13] and Yin et al. [14] exploit the energy bias as the trace to unveil seam carving, which is more closely related to the inherent nature of seam carving. Thus, their detection accuracies are much better than the patch-based method [12] and the BACM-based method [16], especially when the scaling ratios are larger than 10%. However, for those resized images with LSRs, they only achieve average accuracies of 55.94% and 65.72%, respectively. Actually, this is the motivation that we put emphasis on the detection of seam carving with Low LSRs in this paper, simply because it is more challenging. For the proposed detector, it achieves an average accuracy of 85.19% for LSRs. The significant improvement of detection accuracy mainly benefits from the SSE-based features, which are quite sensitive to seam carving, even when the scaling ratios are low. Moreover, since the proposed detector improves the LBP-based energy features [14] by multi-scale images, it also achieves desirable detection accuracies for seam carving with HSRs.

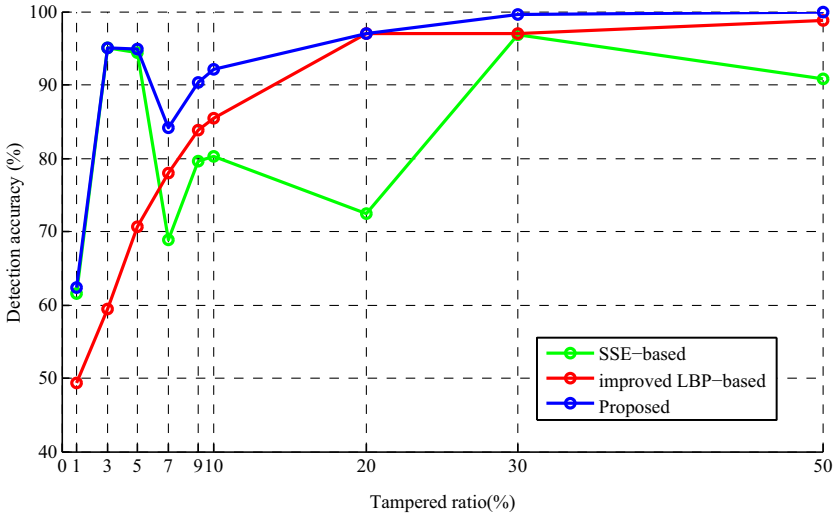

Fig. 10. Effectiveness of SSE-based features and improved LBP-based features.

Fig. 7 shows the ROC curves of five detectors, in which each sub-figure represents the ROC performance under different scaling ratios from 1% to 20%, respectively. The probabilities of true positive (TP) and false positive (FP) are determined with a threshold (ranges from 0 to 1), which is computed by the percentage of correctly classified carved images and the percentage of incorrectly classified non-carved images, respectively. From Fig. 6(a), the true positive rate (TPR) of these five detectors is very low for 1% carved images. With the increase of scaling ratio, the proposed approach achieves much better improvement of ROC performance than the rest four detectors. Compared with the patch-based method [12] and the energy-based method [13], the proposed approach increases the TPR by at least 45% on average with lower false positive rate (FPR) (<0.05). Moreover, because of the SSE-based features over multi-scale images, there is at least 26.67% increase of TPR than the LBP-based method [14]. Actually, the detection precisions presented by these ROC curves are similar with the results reported in Table 4, which further confirms the robustness of the proposed method.

4.2.2. Seam carving with LSCs and further JPEG compression

Digital images are usually saved in JEPG format for storage and transmission. The tampered images after seam carving may be encoded into JPEG images as well. Thus, the proposed detector is also tested for the test image set 2. Table 5 compares the detection accuracies among the LBP-based method [14], the BACM-based method [16] and the proposed approach. The patch-based method [12] and the energy-based method [13] are not compared because they are presented for seam carved forgery detection without further JPEG compression. The best results for each combination (tampered rate, QF) are highlighted in bold as well. From Table 5, it is apparent that the proposed approach achieves the best accuracies for most cases. The exceptions are those tampered images from the UCUS database, which are further compressed into JPEG images with QF100. Under this case, the BACM-based method [16] achieves slightly better accuracies than the proposed approach. However, it is well-known that QF100 is not often used for JPEG compression, since it means the best visual quality after compression and the least saving of storage space as well. Moreover, from Table 5 (c1) and (c2), the detection accuracies of the proposed method are very steady. For a low tampered rate of 5%, the proposed approach still keeps a detection accuracy up to 96.07%. Fig. 8 compares the average accuracies when the resized images are further compressed into JPEG with different QFs. It is apparent that the proposed approach achieves superior performances over the existing approaches. Compared with our earlier LBP-based method [14], the proposed method increases the detection accuracy up to 12% on average. In addition, the performance of the proposed method is independent of database, since the results in Fig. 8(a) are similar to the results in Fig. 8(b). This also confirms the robustness of the proposed approach.

4.2.3. Seam insertion with further JPEG compression

Seam carving can also be used for image enlargement by repeatedly inserting seams. Similar to the discussion in Sarkar's approach [10], we test the performance of the proposed approach against seam insertion with JPEG compression. Experiments are conducted on the test image set 3, and the experimental results are summarized in Table 6. For JPEG compression with high QFs such as QF100, the BACM-based method [16] achieves slightly better performances than the proposed method. When QF is less than 100, the proposed method achieves better performances than [16], especially when the tampered rates are low (less than 10%). When the tamper rate is 1%, the proposed method achieves the accuracies of 98.46% and 97.87% on average for the UCID and UCUS images, respectively. Fig. 9 reports the detection accuracies for the images after seam insertion and JPEG compression with different QFs. When the QFs are less than 100, the proposed approach achieves the best accuracies. Moreover, the proposed approach achieves steadier detection accuracies than the LBP-based method and the BACM-based method.

4.3. Discussion

The proposed approach exploits both the SSE-based features and our earlier LBP-based features. Therefore, their contributions to the overall detection accuracy are also discussed. Fig. 10 compares the detection accuracies by exploiting the SSE-based features, the LBP-based features and both. It is apparent that when the scaling ratio is less than 7%, the detection accuracy mainly comes from the SSE-based features. This confirms our analysis in Section 3. That is, the SSE-based features are sensitive to the local information loss caused by seam carving with LSRs. Meanwhile, we can observe that the LBP-based features are more effective than the SSE-based features for the detection of seam carving with HSRs, because there are more local texture artifacts in this case. When the scaling ratio varies between 7% and 15%, they are actually the critical points of local texture distortion for most images, or

even the critical points of global structural distortion for some images. Thus, the effectiveness of the SSE-based features is decreased, and the effectiveness of the LBP-based features begins to increase. Though there is a drop of the detection accuracy, it is still acceptable because it is more than 84%.

5. Conclusion

Seam carving with LSRs does not leave any visually annoying artifacts, which makes its blind detection very challenging. Since local information loss is the main side effect of seam caving with LSRs, it is also a more feasible clue to expose this forgery. Motivated by this, multi-scale SSE-based features are specifically presented for seam carving forgery detection with LSRs. By considering the fact that users usually do not know the scaling ratio is high or low in blind forensics practice, the forgery detection of seam carving with HSRs is taken into account simultaneously by exploiting the LBP-based features in our earlier work. That is, the SSE-based features (42D) are combined with the LBP-based features (54D) extracted from multi-scale images, and then input into SVM for binary classification. Experimental results show that the proposed approach achieves superior detection performance over state-of-the-art approaches. Meanwhile, it is robust to seam carving with further JPEG compression. However, the detection result is only a binary decision about whether an image has been suffered seam carving or not. For future research, we will attempt to locate tampered regions. Since information loss, local texture distortion and global geometric distortion are the main artifacts of seam carving, more robust features should be designed to reveal the inconsistency of local texture and geometric structure near removed seams [21,22]. Since there are many other CAIR techniques such as patch resizing and non-homogeneous warping [25,26], we will also attempt to further identify the types of various CAIR techniques by designing more generic features from other points of view [27,28] or by exploiting multi-classifier [29–31]. In addition, image entropy can be further investigated from other aspects such as scale space entropy [32,33].

Acknowledgements

This work is supported in part by the National Natural Science Foundation of China (61572183, 61379143, 61672222), the Scientific Research Fund of Hunan Provincial Education Department of China (14C0029,15C0083), Natural Science Foundation of Hunan Province (2016JJ2005, 2017JJ2291).

References

[1] K. Birajdar G, V.H. Mankar, Digital image forgery detection using passive techniques: a survey, Digital Investigat. 10 (3) (2013) 226–245.
[2] A. Qureshi M, M. Deriche, A bibliography of pixel-based blind image forgery detection techniques, Signal Process.: Image Commun. 39 (2015) 46–74.
[3] G. Yang, J. Li, Y. He, et al., An information hiding algorithm based on intra-prediction modes and matrix coding for H.264/AVC video stream, AEU-Int. J. Electron. Commun. 65 (4) (2011) 331–337.
[4] X. Wang, K. Pang, X. Zhou, et al., A visual model-based perceptual image hash for content authentication, IEEE Trans. Inform. Forensics Security 10 (7) (2015) 1336–1349.
[5] J. Li, X. Li, B. Yang, et al., Segmentation-based image copy-move forgery detection scheme, IEEE Trans. Inform. Forensics Security 10 (3) (2015) 507–518.
[6] J. Wang, T. Li, Y.Q. Shi, et al., Forensics feature analysis in quaternion wavelet domain for distinguishing photographic images and computer graphics, Multimedia Tools Appl. doi: http://dx.doi.org/10.1007/s11042-016-4153-0.
[7] S. Avidan, A. Shamir, Seam carving for content-aware image resizing, ACM Trans. Graph. 26 (3) (2007) 10–20.
[8] K. Li, B. Yan, J. Li, et al., Seam carving based aesthetics enhancement for photos, Signal Process.: Image Commun. 39 (2015) 509–516.
[9] Seam carving for content-aware image resizing [EB/OL]. <http://www.faculty.idc.ac.il/arik/SCWeb/imret/index.html> Accessed time: 2016-10-15.
[10] A. Sarkar, L. Nataraj, B.S. Manjunath, Detection of seam carving and localization of seam insertions in digital images, in: Proceedings of the 11th ACM Workshop on Multimedia and Security, 2009, pp. 107–116.
[11] C. Fillion, G. Sharma, Detecting content adaptive scaling of images for forensic applications, IS&T/SPIE Electronic Imaging, International Society for Optics and Photonics, 2010, pp. 75410Z–75410Z.
[12] D. Wei J, J. Lin Y, J. Wu Y, A patch analysis method to detect seam carved images, Pattern Recogn. Lett. 36 (2014) 100–106.
[13] U. Seung-Jin R Y, E. Hae-Yeoun L E, E. Heung-Kyu L E, Detecting trace of seam carving for forensic analysis, IEICE Trans. Inform. Syst. 97 (5) (2014) 1304–1311.
[14] T. Yin, G. Yang, L. Li, et al., Detecting seam carving based image resizing using local binary patterns, Comput. Security 55 (2015) 130–141.
[15] Q. Liu, Z. Chen, Improved approaches with calibrated neighboring joint density to steganalysis and seam-carved forgery detection in JPEG images, ACM Trans. Intell. Syst. Technol. 5 (4) (2014) 63–72.
[16] K. Wattanachote, K. Shih T, L. Chang W, et al., Tamper detection of JPEG image due to seam modifications, IEEE Trans. Inform. Forensics Security 10 (12) (2015) 2477–2491.
[17] C. Hsu C, W. Lin C, Y. Fang, et al., Objective quality assessment for image retargeting based on perceptual geometric distortion and information loss, IEEE J. Select. Top. Signal Process. 8 (3) (2014) 377–389.
[18] R. Sheikh H, C. Bovik A, Image information and visual quality, IEEE Trans. Image Process. 15 (2) (2006) 430–444.
[19] L. Liu, B. Liu, H. Huang, et al., No-reference image quality assessment based on spatial and spectral entropies, Signal Process.: Image Commun. 29 (8) (2014) 856–863.
[20] L. Li, W. Xia, W. Lin, No-reference and robust image sharpness evaluation based on multi-scale spatial and spectral features, IEEE Trans. Multimedia (2016), http://dx.doi.org/10.1109/TMM.2016.2640762.
[21] M. Karimi, S. Samavi, N. Karimi, et al., Quality assessment of retargeted images by salient region deformity analysis, J. Visual Commun. Image Represent. 43 (2017) 108–118.
[22] Y. Zhang, Y. Fang, W. Lin, et al., Backward registration-based aspect ratio similarity for image retargeting quality assessment, IEEE Trans. Image Process. 25 (9) (2016) 4286–4297.
[23] LibSVM: a library for support vector machines [EB/OL]. <http://www.csie.ntu.edu.tw/cjlin/libsvm/> Accessed time: 2016-11-12.
[24] UCID: an uncompressed color image database [EB/OL]. <http://homepages.lboro.ac.uk/cogs/datasets/ucid/ucid.html> Accessed time: 2016-11-12.
[25] S. Lin S, C. Yeh I., H. Lin C, et al., Patch-based image warping for content-aware retargeting, IEEE Trans. Multimedia 15 (2) (2013) 359–368.
[26] Y. Niu, F. Liu, X. Li, et al., Image resizing via non-homogeneous warping, Multimedia Tools Appl. 56 (3) (2012) 485–508.
[27] Z. Zhou, Y. Wang, Q.M.J. Wu, et al., Effective and efficient global context verification for image copy detection, IEEE Trans. Inform. Forensics Security 12 (1) (2017) 48–63.
[28] Z. Xia, X. Wang, X. Sun, et al., Steganalysis of LSB matching using differences between nonadjacent pixels, Multimedia Tools Appl. 75 (4) (2016) 1947–1962.
[29] B. Gu, S. Sheng V., Y. Tay K, et al., Incremental support vector learning for ordinal regression, IEEE Trans. Neural Netw. Learning Syst. 26 (7) (2015) 1403–1416.
[30] B. Gu, X. Sun, V.S. Sheng, Structural minimax probability machine, IEEE Trans. Neural Netw. Learning Syst. 28 (7) (2017) 1646–1656.
[31] B. Gu, V.S. Sheng, A robust regularization path algorithm for ν-support vector classification, IEEE Trans. Neural Netw. Learning Syst. 28 (5) (2017) 1241–1248.
[32] Y. Wu, Y. Zhou, G. Saveriades, et al., Local Shannon entropy measure with statistical tests for image randomness, Inform. Sci. 22 (2013) 323–342.
[33] M. Ferraro, G. Boccignone, T. Caelli, On the representation of image structures via scale space entropy conditions, IEEE Trans. Pattern Anal. Machine Intell. 21 (11) (1999) 1199–1203,.